ELSEVIER

Contents lists available at ScienceDirect

Extreme Mechanics Letters

journal homepage: www.elsevier.com/locate/eml





Acoustic chiral mode transfer for symmetry-broken states in anti-parity-time symmetric systems

Youdong Duan ^a, Lei Zhang ^a, Yonghui Zhang ^a, Linlin Geng ^a, Qiuquan Guo ^b, Jun Yang ^b, Gengkai Hu ^a, Xiaoming Zhou ^a,*

- ^a Key Laboratory of Dynamics and Control of Flight Vehicle of Ministry of Education, School of Aerospace Engineering, Beijing Institute of Technology, Beijing, 100081, China
- b ShenSi Lab, Shenzhen Institute for Advanced Study, University of Electronic Science and Technology of China, Shenzhen, 518110, China

ARTICLE INFO

Keywords: Non-Hermitian acoustics Exceptional point Anti-parity-time symmetry Coupled mode theory Chiral mode transfer

ABSTRACT

Dynamic encircling of an anti-parity-time (anti-PT) symmetric exceptional point (EP) leads to chiral transfer of symmetry-broken modes, which has been explored in various systems except acoustics. In this work, acoustic counterpart of this behavior is numerically demonstrated in coupled waveguide systems with anti-PT-symmetric EPs. The model consists of three coupled waveguides designed to mimic a three-state system that can be described by the coupled mode theory. By adiabatically eliminating the intermediate state with high loss, the anti-PT symmetry and associated EP can be formed in an effective system comprising the remaining two states. According to the parametric path enclosing the EP, acoustic propagation model is designed to support the space-driven acoustic mode evolution. Numerical simulations are conducted to demonstrate acoustic chiral transfer of symmetry-broken states.

1. Introduction

Nonconservative mechanical systems that could exchange energy with surroundings can be characterized by non-Hermitian Hamiltonians. In particular, the Hamiltonian with the parity-time (PT) symmetry, appearing usually in gain/loss balanced systems, possesses degeneracy singularities called exceptional points (EPs), where eigenvalues and eigenvectors coalesce simultaneously [1,2]. In recent years, PTsymmetric EPs have been widely explored in various physical platforms including acoustic [3-5], elastodynamic [6,7], microwave [8,9], and photonic [10,11] systems, and many intriguing phenomena associated to EPs have been found ranging from enhanced sensing [12,13], unidirectional non-reflection [14,15], to coherent perfect absorption and lasing [16-18], etc. In addition, due to the existence of selfintersecting eigenvalue Riemann surface near EPs, dynamic encircling of PT-symmetric EPs in parameter space can lead to chiral mode switching of symmetric-phase modes [19,20], which can be exploited for unusual wave mode control.

The Hamiltonian with anti-PT symmetry is another scenario that has received considerable attention. In contrast to PT-symmetric systems, the anti-PT-symmetric Hamiltonian requires two eigenstates interacted with the purely imaginary coupling for a two-state system [21,22], and it also supports the occurrence of EPs, yet the eigenvalue Riemann surface would be reversed. Thereby, the phenomenon associated

to symmetric-phase modes in PT-symmetric systems can be immigrated to symmetry-broken states in anti-PT-symmetric systems. For example, dynamic encircling of anti-PT-symmetric EPs would lead to chiral mode switching of symmetry-broken states, as demonstrated in mechanical [23], microwave [24] and optical [25,26] systems. The symmetry-broken states may be of more interest in wave mode control since each eigenmode is localized in sub-systems only and can be used directly as the input and output channels.

Chiral mode switching of symmetry-broken states induced by the anti-PT symmetry has not been demonstrated in acoustic systems despite the broad exploration of relevant phenomena in other platforms. In our previous study, coupled waveguide systems are proposed to realize acoustic chiral mode switching of symmetric-phase modes via the space-driven dynamic encircling of an EP [27]. In this work, the waveguide model is extended from the following aspects to engineer the chiral transfer of symmetry-broken states. Firstly, three coupled waveguides are designed to mimic a three-state system, where the intermediate state with high loss is reduced by the adiabatic elimination such that the remaining two states constitute an effective anti-PT-symmetric system with EPs. Secondly, the condition for constructing anti-PT-symmetric EPs is given, and then used to design a waveguide

E-mail addresses: genglinlin@bit.edu.cn (L. Geng), zhxming@bit.edu.cn (X. Zhou).

^{*} Corresponding author.

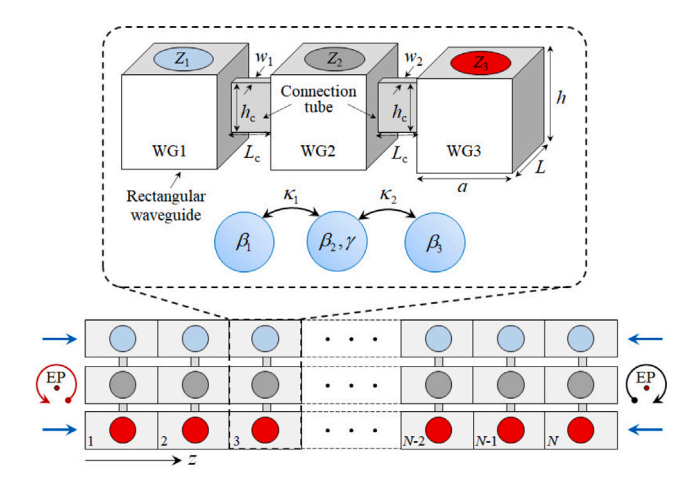


Fig. 1. Schematic diagram of a three-state waveguide system, where the intermediate waveguide WG2 involves high losses, and after adiabatically eliminated, WG1 and WG3 constitute an effective two-state system with the anti-PT symmetry.

system to support the space-propagation acoustic mode evolution enclosing the EP. Based on the developed acoustic model, chiral dynamics of symmetry-broken states is demonstrated by numerical simulations.

2. Construction of anti-PT-symmetric EPs

Consider three rectangular waveguides with identical geometries of height h, width a, and length L, as shown in Fig. 1. They host three fundamental propagation modes that constitute a three-state system. Acoustic impedance boundaries Z_1 , Z_2 and Z_3 that cover a circular area of radius R are introduced to manipulate the wave vectors of each waveguide (WG1, WG2 and WG3) as represented by β_1 , $\beta_2 - i\gamma$ and β_3 , respectively. Notice that the decaying factor γ specially introduced into WG2 is key to create the purely imaginary coupling as required by the anti-PT symmetry. Adjacent waveguides are coupled through narrow tubes of sizes h_c , L_c , w_1 , and w_2 . Denote acoustic pressure fields in three waveguides by A_k (k=1,2,3). Acoustic propagation in coupled waveguide system can be described by the spatial coupled-mode equation

$$i\frac{\mathrm{d}}{\mathrm{d}z}\Psi(z) = \mathbf{H}\Psi(z), \quad \mathbf{H} = \begin{bmatrix} \beta_1 & \kappa_1 & 0\\ \kappa_1 & \beta_2 - i\gamma & \kappa_2\\ 0 & \kappa_2 & \beta_3 \end{bmatrix}$$
(1)

where $\Psi(z) = \left[A_1(z), A_2(z), A_3(z)\right]^T$. The off-diagonal terms κ_1 and κ_2 in the Hamiltonian matrix **H** describes the coupling magnitude between adjacent waveguides, and is dominated by the connection tube. The relationship between Hamiltonian and structural parameters can be established by using the fitting method as briefly described below, while the details can be found in the Supplementary Material.

Denote eigenvalues of the Hamiltonian **H** by λ_n (n=1,2,3). Pressure fields $A_k(z)$ in each waveguide can be expressed as a linear combination of eigenmodes

$$A_k(z) = \sum_{n=1}^3 a_{kn} e^{-i\lambda_n z} \tag{2}$$

where a_{kn} (k,n=1,2,3) are unknown coefficients. By substituting Eq. (2) into first two equations of (1), it can be derived that $c_n=d_n=0$, where

$$\begin{cases} c_n = \lambda_n a_{1n} - \beta_1 a_{1n} - \kappa_1 a_{2n} \\ d_n = -\kappa_1 a_{1n} + (\lambda_n - \beta_2 + i\gamma) a_{2n} - \kappa_2 a_{3n} \end{cases}$$
(3)

According to Eq. (2), acoustic pressures at the boundary z=0 are given by $A_k(0)=a_{k1}+a_{k2}+a_{k3}$, where $A_k(0)$ are boundary conditions applied to the entrance port of the z_1 -element, and set as $A_{1,3}(0)=0$ and $A_2(0)=0$

1. Based on the conditions given above, a_{kn} can be calculated, and then the analytic expression of $A_k(z)$ can be obtained. All Hamiltonian parameters in **H** can be determined by fitting the expression of $A_k(z)$ with simulation results of pressure fields.

Perform adiabatic elimination [28,29] of the wave mode hosted by the intermediate waveguide (WG2) (see Supplementary Material for details). Under conditions of $\gamma \gg \kappa_{1,2}$ and $\gamma \gg \Delta \beta_{1,3}$ with $\Delta \beta_{1,3} = \beta_{1,3} - \beta_2$, wave modes supported by WG1 and WG3 constitute an effective two-state system, which satisfies the following coupled-mode equation $i\frac{\mathrm{d}}{\mathrm{d}z}\Phi(z) = \mathbf{H}_{\mathrm{A}}\Phi(z) \tag{4}$

where $\Phi(z) = [A_1(z), A_3(z)]^T$, and

$$\mathbf{H}_{\mathbf{A}} = \begin{bmatrix} \beta_1 + i\Gamma_{11} & i\Gamma_{12} \\ i\Gamma_{21} & \beta_3 + i\Gamma_{22} \end{bmatrix}$$
 (5)

with $\Gamma_{11}=\kappa_1^2/\left(i\Delta\beta_1-\gamma\right)$, $\Gamma_{12}=\kappa_1\kappa_2/\left(i\Delta\beta_3-\gamma\right)$, $\Gamma_{21}=\kappa_1\kappa_2/\left(i\Delta\beta_1-\gamma\right)$ and $\Gamma_{22}=\kappa_2^2/\left(i\Delta\beta_3-\gamma\right)$. By solving the eigenvalue problem of Eq. (4), the EP condition, which corresponds to the simultaneous coalescence of eigenvalues and eigenvectors, can be theoretically derived. When the adiabatic elimination condition $\gamma\gg\Delta\beta_{1,3}$ is guaranteed, it can be found from Eq. (5) that the coupling terms $i\Gamma_{12}$ and $i\Gamma_{21}$ in \mathbf{H}_{A} are purely imaginary values, which are signatures of the anti-PT-symmetric system [22,30]. Further analyses are given below by numerical examples.

According to the EP condition and adiabatic elimination approximation, the coupled-waveguide system that supports the EP can be designed. As an example, an EP system is designed with the following structural parameters: h=1.6 cm, a=1 cm, L=3 cm, $h_c=0.4$ cm, $L_c=0.3$ cm, $w_1=0.37$ mm, $w_2=0.22$ mm and R=0.4 cm. Acoustic impedances are $Z_1=16.41i\rho_0c_0$, $Z_2=(4.47-0.7i)\rho_0c_0$ and $Z_3=9.9i\rho_0c_0$, where the air density and sound velocity are $\rho_0=1.21$ kg/m³ and $c_0=343$ m/s, respectively. Notice that these impedance conditions are practically realizable using loudspeakers with shunting circuits [14,31]. Acoustic excitation frequency is f=8 kHz. The Hamiltonian parameters of this EP system are $\beta_1=145.9$ rad/m, $\beta_2=146.1$ rad/m, $\beta_3=145.8$ rad/m, $\gamma=1.16$ rad/m, $\kappa_1=0.265$ rad/m and $\kappa_2=0.21$ rad/m.

Figs. 2(a) and 2(b) show imaginary and real parts of eigenvalues λ near the EP as calculated by Eq. (1) for various κ_1 and κ_2 , while other Hamiltonian parameters remain unchanged. It is seen from Fig. 2(a) that the imaginary part pattern comprises three spectrum sheets with low (blue), high (red) and extremely high (gray) losses, here termed as L, H, and K modes, respectively. Imaginary parts of eigenvalues of L and H modes coalesce in a line where their real parts are different. Fig. 2(c) shows this coalescing line in the parameter space (κ_1, κ_2) , where the structural system for a specific point (A) has been designed with the modal field displayed in the inset. The energy localization in either the waveguide WG1 or WG3 can be observed, which is the typical feature of the anti-PT-broken phase. Real parts of eigenvalues of L and H modes are characterized by self-intersecting Riemann surfaces, and they coalesce at the anti-PT-symmetric phase line since the energy is evenly distributed between waveguides WG1 and WG3, as validated by the modal field at point B in Fig. 2(c). The EP locates at the intersecting point between the symmetric-phase and broken-phase lines. Same modal fields for L and H modes at EP can be observed. demonstrating the degeneracy of eigenvectors. It can be seen from Fig. 2(c) that the energy localization distribution is changed to the balancing one when the broken state evolves into the coalescing state at EP. After passing through the EP, the eigenstate is changed to the symmetric-phase mode, where the balancing distribution between WG1 and WG3 is preserved, while a small portion of energy is localized in the WG2 for the H mode. The coalescing modal fields at EP is seen to play a central role in the mode evolution from broken to symmetry states. Above features are in accordance with those in anti-PT-symmetric systems [22,23], and the EP, at which two characteristic lines intersect, is usually called the anti-PT-symmetric exceptional point

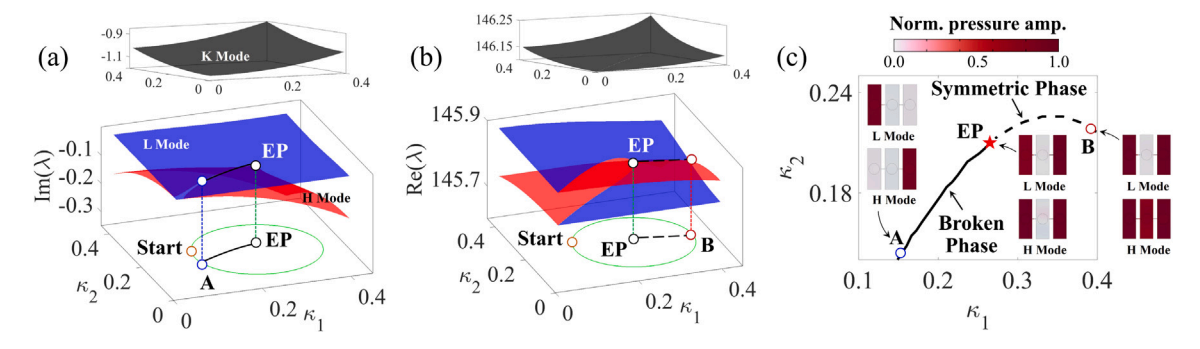


Fig. 2. (a) Imaginary and (b) real parts of eigenvalues λ of the three-state waveguide system in the parameter space (κ_1, κ_2) ; (c) EP and the lines of anti-PT symmetric and broken phase together with their typical modal fields for L and H modes. (For interpretation of the references to color in this figure legend, the reader is referred to the web version of this article.)

to distinguish the case in PT-symmetric systems [19,32]. Notice that the K mode possesses a sufficiently large damping positioned away from L and H modes, thus can be adiabatically eliminated to form the anti-PT symmetry.

3. Chiral transfer of symmetry-broken states

Dynamic encircling of the anti-PT-symmetric EP can result in the chiral transfer of symmetry-broken states [22–24]. Acoustic counterpart of this behavior would be demonstrated in the proposed model. The parametric path enclosing the EP with the starting point near the anti-PT-broken phase is chosen as

$$\begin{cases} \kappa_1(z) = 0.14\cos\phi(z) + 0.265\\ \kappa_2(z) = 0.14\sin\phi(z) + 0.21 \end{cases}$$
 (6)

where $\phi(z) = 2\pi z/L_t - 0.9\pi$, and L_t refers to the wave propagation length in a complete evolution enclosing the EP. To design the waveguide system that supports acoustic mode evolution, the loop trajectory as described by Eq. (6) is discretized into N = 1100 parametric points positioned at $z_i = (j-1)L$ (j = 1,...,N). N waveguide elements are designed separately to fulfill parameter conditions of $\kappa_1(z_i)$ and $\kappa_2(z_i)$ by using the fitting method, and then stacked in order along the z direction such that acoustic propagation in the waveguide is equivalent to the dynamic encircling of the anti-PT-symmetric EP. Fig. 3 illustrates the coupling magnitudes $\kappa_{1,2}$ used for implementing the dynamic encircling of the EP, and their relationships with the widths $w_{1,2}$ of connection tubes, where the tube height h_c and length $L_{\rm c}$ are kept unchanged. The good agreement between $\kappa_{1,2}$ and $w_{1,2}$ can be seen, stating the dominant role of the tube width in tuning the state coupling. Wave traveling along the positive and negative z direction corresponds to the anti-clockwise and clockwise encircling of the EP, respectively. Methods for numerical simulation of acoustic propagation evolution of anti-PT-broken states and to retrieve modal amplitudes $q_{\rm L}$, $q_{\rm H}$ and $q_{\rm K}$ for L, H and K modes respectively are similar to the strategies adopted in PT-symmetric waveguide systems [27], but extended to the three-state scenarios as detailed in the Supplementary Material.

Fig. 4 shows the variation of modal amplitudes $q_{\rm L}$, $q_{\rm H}$ and $q_{\rm K}$ in the process of dynamic encircling of the EP for different loop directions and input states. The anti-clockwise evolution is implemented by injecting acoustic energy into the z_1 -element of the system, as shown in Figs. 4(a) and 4(b) for H and L input modes, respectively. It is observed that two input modes are soon transformed into each other owing to the branch cut (BC), which can induce the exchange of mode identity according to eigenvalue properties [23,27]. The transformed state, if dominated by the H mode as is the case in Fig. 4(b), decays faster upon the wave propagation along z than the L dominant mode because the H mode is adhered with higher losses. As a result, its amplitude intersects with the L mode curve after some propagation distance, forming the non-adiabatic transition (NAT) [33], and then the L mode becomes dominant at the end of evolution. When the L mode is dominant at

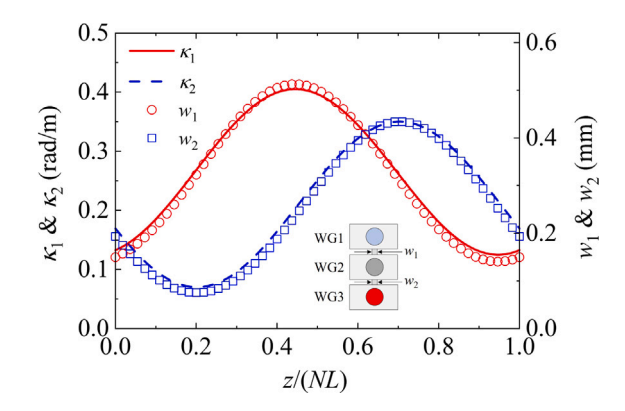


Fig. 3. The coupling magnitudes $\kappa_{1,2}$ for implementing the dynamic encircling of the EP, and their relationships with the widths $w_{1,2}$ of connection tubes.

the early stage of evolution, its amplitude decays slowly and keeps separated with the H mode curve without the occurrence of the NAT, and finally, the system outputs the L mode as shown in Fig. 4(a). Fig. 4(c,d) show the results of the clockwise encircling case realized by inputting acoustic energy to the z_N -element. It is seen that the input H mode is firstly converted to the L mode due to the NAT, and then returns back to the H mode after crossing the BC. The input L mode propagates without inducing the NAT, but eventually changed to the H mode by the BC. In all cases, the K mode with near-zero modal amplitudes remains almost not interacting with H and L modes, as guaranteed by adiabatic elimination. Theoretical results of modal amplitudes predicted by Eq. (1) have also been provided in Fig. 4, and are in good agreement with simulation results. Results in Fig. 4 clearly demonstrate the chiral transfer of symmetry-broken states with the L (H) mode outputted from the anti-clockwise (clockwise) encircling of the anti-PT-symmetric EP regardless of input states.

Chiral dynamics of symmetry-broken states can be also validated by analyzing pressure amplitudes of input and output elements. The start/end points locate near the anti-PT-broken phase, where the energy is localized in either WG1 or WG3 corresponding respectively to the L or H mode as disclosed in Fig. 2(c). Thus, the output mode at the end of evolution can be distinguished based on wave amplitudes. Fig. 5 shows pressure amplitudes $|p_1|$, $|p_2|$ and $|p_3|$ in waveguides WG1, WG2 and WG3, respectively, associated to four cases in Fig. 4. It can be observed that the dynamic encircling of the anti-PT-symmetric EP ends with the energy localization in WG1 for the anti-clockwise evolution, which corresponds to the L mode, while in WG3 for the clockwise case as controlled by the H mode, demonstrating again acoustic chiral mode transfer of symmetry-broken states.

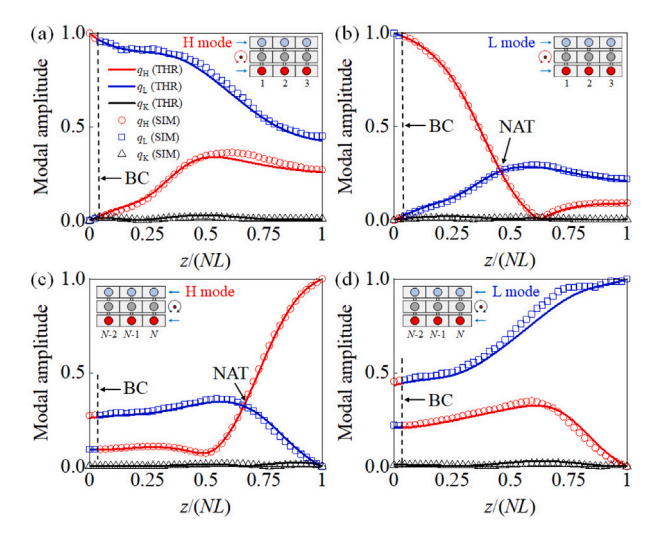


Fig. 4. Simulation (SIM) and theoretical (THR) results of modal amplitudes $q_{\rm L}$, $q_{\rm H}$ and $q_{\rm K}$ for L, H and K modes respectively in the process of dynamic encircling of the anti-PT-symmetric EP for different input states and evolution directions: (a) H mode input and anti-clockwise evolution; (b) L mode input and anti-clockwise evolution; (c) H mode input and clockwise evolution;

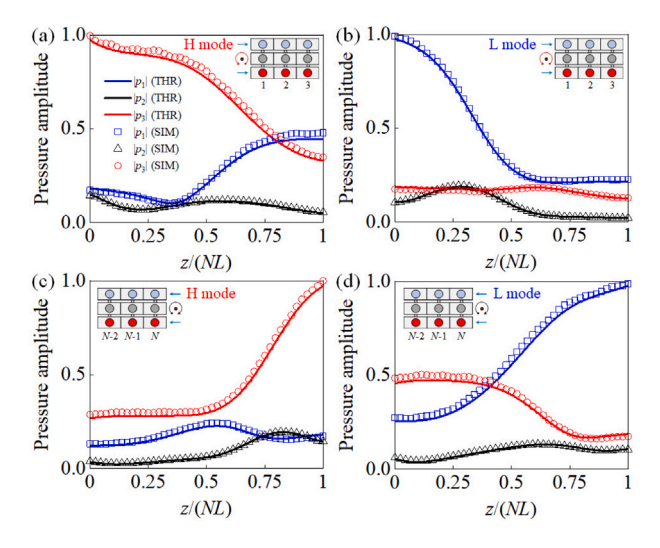


Fig. 5. (a–d) Simulation (SIM) and theoretical (THR) results of pressure amplitudes $|p_1|$, $|p_2|$ and $|p_3|$ in waveguides WG1, WG2 and WG3, corresponding to four cases in Fig. 4(a–d) respectively.

4. Summary

Acoustic coupled waveguide system provides a versatile platform for exploring the non-adiabatic coupling and evolution phenomena of sounds [27]. In this work, the coupled waveguide model is extended to design non-Hermitian acoustic systems with the anti-PT symmetric EP. The strategy to create the anti-PT symmetry is based on the adiabatic elimination of the intermediate state with high loss in a three-state waveguide system. According to the loop trajectory enclosing the EP, acoustic propagation model is devised to implement the dynamic evolution of symmetry-broken states, and the chiral mode transfer behavior is observed by numerical simulations, which are in good agreement with the prediction by the coupled mode theory. Symmetry-broken modes are characterized by the energy localization in individual waveguides, which can be used directly as the input and output channels. Thus, the chiral transfer control of these modes may be of significance for device applications in signal processing and communication of sounds.

CRediT authorship contribution statement

Youdong Duan: Writing – original draft, Methodology, Investigation, Conceptualization. Lei Zhang: Validation, Methodology, Investigation. Yonghui Zhang: Validation, Methodology, Investigation. Linlin Geng: Writing – original draft, Validation, Methodology, Investigation. Qiuquan Guo: Writing – review & editing, Validation. Jun Yang: Writing – review & editing, Validation. Gengkai Hu: Writing – review & editing, Validation. Xiaoming Zhou: Writing – review & editing, Validation, Supervision, Methodology, Investigation, Conceptualization.

Declaration of competing interest

The authors declare that they have no known competing financial interests or personal relationships that could have appeared to influence the work reported in this paper.

Acknowledgments

This work was supported by the National Natural Science Foundation of China (12225203, 11622215, 11872111, 11991030, and 11991033), 111 Project, China (B16003), and Guangdong Basic and Applied Basic Research Foundation, China (2021A1515110880).

Appendix A. Supplementary data

Supplementary material related to this article can be found online at https://doi.org/10.1016/j.eml.2024.102261.

Data availability

Data will be made available on request.

References

- Changqing Wang, Zhoutian Fu, Wenbo Mao, Jinran Qie, Douglas Stone, Lan Yang, Non-Hermitian optics and photonics: from classical to quantum, Adv. Opt. Photon. 15 (2) (2023) 442–523.
- [2] Aodong Li, Heng Wei, Michele Cotrufo, Weijin Chen, Sander Mann, Xiang Ni, Bingcong Xu, Jianfeng Chen, Jian Wang, Shanhui Fan, Cheng-Wei Qiu, Andrea Alu, Lin Chen, Exceptional points and non-Hermitian photonics at the nanoscale, Nat. Nanotechnol. 18 (7) (2023) 706–720.
- [3] Kun Ding, Guancong Ma, Meng Xiao, Z.Q. Zhang, C.T. Chan, Emergence, coalescence, and topological properties of multiple exceptional points and their experimental realization, Phys. Rev. X. 6 (2) (2016) 021007.
- [4] Chengzhi Shi, Marc Dubois, Yun Chen, Lei Cheng, Hamidreza Ramezani, Yuan Wang, Xiang Zhang, Accessing the exceptional points of parity-time symmetric acoustics, Nat. Commun. 7 (2016) 11110.
- [5] Weiwei Zhu, Xinsheng Fang, Dongting Li, Yong Sun, Yong Li, Yun Jing, Hong Chen, Simultaneous observation of a topological edge state and exceptional point in an open and non-Hermitian acoustic system, Phys. Rev. Lett. 121 (12) (2018) 124501.
- [6] Renan L. Thomes, Matheus I.N. Rosa, Alper Erturk, Experimental realization of tunable exceptional points in a resonant non-Hermitian piezoelectrically coupled waveguide, Appl. Phys. Lett. 124 (6) (2024) 061702.
- [7] Yabin Jin, Wenjun Li, Bahram Djafari-Rouhani, Yan Li, Yanxun Xiang, Exceptional points for crack detection in non-Hermitian beams, J. Sound Vib. 572 (2024) 118162.
- [8] Dengke Zhang, Xiao-Qing Luo, Yi-Pu Wang, Tie-Fu Li, J.Q. You, Observation of the exceptional point in cavity magnon-polaritons, Nat. Commun. 8 (2017) 1368.
- [9] Jae Woong Yoon, Youngsun Choi, Choloong Hahn, Gunpyo Kim, Seok Ho Song, Ki-Yeon Yang, Jeong Yub Lee, Yongsung Kim, Chang Seung Lee, Jai Kwang Shin, Hong-Seok Lee, Pierre Berini, Time-asymmetric loop around an exceptional point over the full optical communications band, Nature 562 (7725) (2018) 86–90.
- [10] Alois Regensburger, Christoph Bersch, Mohammad-Ali Miri, Georgy Onishchukov, Demetrios N. Christodoulides, Ulf Peschel, Parity-time synthetic photonic lattices, Nature 488 (7410) (2012) 167–171.
- [11] Mohammad-Ali Miri, Andrea Alu, Exceptional points in optics and photonics, Science 363 (6422) (2019) eaar7709.

- [12] Tong Xing, Ziwen Pan, Yu Tao, Guohui Xing, Rong Wang, Wenyao Liu, Enbo Xing, Jiamin Rong, Jun Tang, Jun Liu, Ultrahigh sensitivity stress sensing method near the exceptional point of parity-time symmetric systems, J. Phys. D-Appl. Phys. 53 (20) (2020) 205102.
- [13] Jinbo Yuan, Linlin Geng, Jiahui Huang, Qiuquan Guo, Jun Yang, Gengkai Hu, Xiaoming Zhou, Exceptional points induced by time-varying mass to enhance the sensitivity of defect detection, Phys. Rev. Appl. 18 (6) (2022) 064055.
- [14] R. Fleury, D. Sounas, A. Alù, An invisible acoustic sensor based on parity-time symmetry, Nat. Commun. 6 (2015) 5905.
- [15] Yin Huang, Yuecheng Shen, Changjun Min, Shanhui Fan, Georgios Veronis, Unidirectional reflectionless light propagation at exceptional points, Nanophotonics 6 (5) (2017) 977–996.
- [16] Changqing Wang, William R. Sweeney, A. Douglas Stone, Lan Yang, Coherent perfect absorption at an exceptional point, Science 373 (6560) (2021) 1261–1265.
- [17] Yong Sun, Wei Tan, Hong-qiang Li, Jensen Li, Hong Chen, Experimental demonstration of a coherent perfect absorber with PT phase transition, Phys. Rev. Lett. 112 (14) (2014) 143903.
- [18] Runcheng Cai, Yabin Jin, Yong Li, Jie Zhu, Hehua Zhu, Timon Rabczuk, Xiaoying Zhuang, Absorption-lasing effects and exceptional points in parity-time symmetric non-Hermitian metaplates, J. Sound Vib. 555 (2023) 117710.
- [19] Xu Lin Zhang, Shubo Wang, Bo Hou, C.T. Chan, Dynamically encircling exceptional points: In situ control of encircling loops and the role of the starting point, Phys. Rev. X. 8 (2) (2018) 021066.
- [20] Linlin Geng, Weixuan Zhang, Xiangdong Zhang, Xiaoming Zhou, Topological mode switching in modulated structures with dynamic encircling of an exceptional point, Proc. R. Soc. A. 477 (2245) (2021) 20200766.
- [21] Y. Yang, Yi-Pu Wang, J.W. Rao, Y.S. Gui, B.M. Yao, W. Lu, C.-M. Hu, Unconventional singularity in anti-parity-time symmetric cavity magnonics, Phys. Rev. Lett. 125 (14) (2020) 147202.
- [22] Xu-Lin Zhang, Tianshu Jiang, C.T. Chan, Dynamically encircling an exceptional point in anti-parity-time symmetric systems: asymmetric mode switching for symmetry-broken modes, Light-Sci. Appl. 8 (2019) 88.

- [23] Linlin Geng, Weixuan Zhang, Xiangdong Zhang, Xiaoming Zhou, Chiral mode transfer of symmetry-broken states in anti-parity-time-symmetric mechanical system, Proc. R. Soc. A. 477 (2256) (2021) 20210641.
- [24] Chaowei Sui, Mingyu Ma, Shaohua Yuan, Jie Zheng, Daqiang Gao, Vladimir Koval, Chenglong Jia, Dynamically encircling an exceptional point by microwave fields in synthetic antiferromagnets, Phys. Rev. B 108 (21) (2023) 214420.
- [25] Ziyao Feng, Xiankai Sun, Harnessing dynamical encircling of an exceptional point in anti-PT-symmetric integrated photonic systems, Phys. Rev. Lett. 129 (27) (2022) 273601.
- [26] Weiwei Liu, Yicong Zhang, Zhihua Deng, Jianghua Ye, Kai Wang, Bing Wang, Dingshan Gao, Peixiang Lu, On-chip chiral mode switching by encircling an exceptional point in an anti-parity-time symmetric system, Laser Photon. Rev. 16 (12) (2022).
- [27] Youdong Duan, Linlin Geng, Qiuquan Guo, Jun Yang, Gengkai Hu, Xiaoming Zhou, Acoustic chiral mode switching by dynamic encircling of exceptional points, Appl. Phys. Lett. 123 (10) (2023) 101701.
- [28] A. Hashemi, S.M. Rezaei, S.K. Ozdemir, R. El-Ganainy, New perspective on chiral exceptional points with application to discrete photonics, APL Photon. 6 (4) (2021) 040803.
- [29] Michael Mrejen, Haim Suchowski, Taiki Hatakeyama, Chihhui Wu, Liang Feng, Kevin O'Brien, Yuan Wang, Xiang Zhang, Adiabatic elimination-based coupling control in densely packed subwavelength waveguides, Nat. Commun. 6 (2015) 7565
- [30] Fan Yang, Yong-Chun Liu, Li You, Anti-PT symmetry in dissipatively coupled optical systems, Phys. Rev. A 96 (5) (2017) 053845.
- [31] Yu Huang, Xiaoming Zhou, Non-reciprocal sound transmission in electro-acoustic systems with time-modulated circuits, Acta Mech. Solida Sin. 35 (6) (2022) 940–948.
- [32] S.K. Ozdemir, S. Rotter, F. Nori, L. Yang, Parity-time symmetry and exceptional points in photonics, Nat. Mater. 18 (8) (2019) 783–798.
- [33] Eva-Maria Graefe, Alexei A. Mailybaev, Nimrod Moiseyev, Breakdown of adiabatic transfer of light in waveguides in the presence of absorption, Phys. Rev. A 88 (3) (2013) 033842.